Polymer 328 (2025) 128406

Contents lists available at ScienceDirect

Polymer

journal homepage: www.elsevier.com/locate/polymer

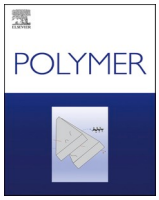

Unique properties of flow-drawn epoxy fibers

Israel Greenfeld *, Mark Shneider, Ulyana Shimanovich, H. Daniel Wagner

Department of Molecular Chemistry and Materials Science, Weizmann Institute of Science, Rehovot, 76100, Israel

A R T I C L E I N F O

Keywords:
Thermoset
Polymer
Epoxy
Fiber
Stiffness
Strength
Ductility
Extensional flow
Electrospinning
Drawing

A B S T R A C T

Epoxy micro and nano fibers prepared from a solution by extensional flow, using newly-developed mechanical and electrical drawing techniques, were recently shown to exhibit remarkable mechanical stiffness. In the current study, we investigate the ultimate strength and ductility of these fibers. The flow-induced high extension is shown to increase these properties well beyond those of bulk epoxy because of the molecular orientation and rearrangement of branching polymer clusters. At the same time, due to volume conservation and tighter molecular packing, when the extension is increased the fiber diameter gets progressively smaller. The mechanical properties are predicted to correlate with the fiber diameter via inverse-square power laws, reflecting the simultaneous molecular alignment and diameter shrinkage. This size-dependence phenomenon starts at a critical diameter, unique to the resin composition and drawing conditions, leading to a steep rise in strength and stiffness for fiber diameters thinner than the critical diameter. The strength and ductility analysis is corroborated by experimental testing of epoxy fibers prepared by extensional flow and may apply to other thermoset polymers, demonstrating the potential to manipulate mechanical properties by controlling the curing and drawing processes.

1. Introduction

Thermosetting polymers such as epoxy are synthesized through a curing process where liquid resin undergoes irreversible, covalent bonding (crosslinking) between monomers. In contrast to thermoplastic polymers, which lack crosslinks and are instead composed of reversibly entangled long chains, thermosets cannot be reshaped or melted once cured. The extensive crosslinking forms a three-dimensional network throughout the cured material, imparting strength, hardness, stiffness, high-temperature resistance, and chemical resilience [1]. However, due to rigidity, most thermosets tend to be brittle and prone to fracture. Epoxy resins represent a notable class within thermoset polymers. Their monomers feature epoxide end-groups, which react with hardeners like polyfunctional amines, fostering robust cross-linkages with neighboring epoxy units. Epoxy is widely used in applications spanning structural and engineering adhesives, electronics encapsulation, protective coatings, films, and sealing; it is found in aircraft and satellites as a composite matrix reinforced with glass and carbon fibers [2,3].

Recent utilization of extensional flow techniques in making micro and nano-scale thermoset polymer fibers (Fig. 1a and b) has unveiled remarkable phenomenological and mechanical properties. For example, the stiffness, ultimate strength, plastic ductility, and toughness of epoxy fibers are much higher compared to bulk epoxy (Fig. 1c). Stiffness is the material resistance to elastic deformation, quantified by Young's modulus, the slope of the stress-strain curve in the elastic region. Strength is the material resistance to failure under load, quantified by the maximum (ultimate) stress it can endure before breaking. Ductility is the material ability to deform plastically, measured by the amount of plastic strain it can withstand before breaking. Toughness is the material ability to resist crack propagation, indicating its capacity to absorb energy before fracturing.

Epoxy fibers exhibit a striking change in structural behavior from the brittle state of bulk epoxy to a ductile state (brittle-ductile transition), implying a significant alteration in their internal molecular and supramolecular conformation. Notably, below a specific critical diameter, epoxy microfibers demonstrate significantly enhanced stiffness, strength, and toughness as their diameter gradually decreases [4–10]. This phenomenon, sometimes termed size effect, has been thoroughly investigated in thermoplastic nanofibers using several theoretical models, including surface tension, confinement, molecular orientation, crystallinity, and density grading [11,12]. However, its exploration in thermosets remains limited.

The investigation of thermoset micro and nanofibers prepared by extensional flow is relatively novel, employing techniques such as

* Corresponding author.
E-mail addresses: green_is@netvision.net.il (I. Greenfeld), Daniel.Wagner@weizmann.ac.il (H.D. Wagner).

https://doi.org/10.1016/j.polymer.2025.128406
Received 18 December 2024; Received in revised form 12 April 2025; Accepted 13 April 2025
Available online 14 April 2025

electrical drawing (electrospinning) and mechanical drawing (pulling) of polymer solutions or neat resin. Extensional flow is characterized by external forces that generate a streaming jet of gradually increasing velocity and decreasing diameter (Fig. 1a); the rate by which the velocity increases is the velocity gradient, or strain rate (denoted by s), that causes the stretching of the jet. Subjected to such a flow, a polymer chain segment experiences higher velocity in its down-stream part than in its up-stream part, and this velocity difference causes chain stretching and alignment with the stream. The resulting molecular orientation has a significant, positive impact on the fibers' mechanical properties.

Only recently was a model suggested that explains the effect of extensional flow on thermoset fibers' molecular conformation and stiffness [13]. Although molecular elongation under extensional flow has been extensively studied in thermoplastic polymers [14–18] using concepts like linear flexible chains, entanglement, confining tube, chain reptation, and chain stretching and retraction [12,19–27], the unique characteristics of thermoset polymers necessitate distinct modeling approaches. Thermosets are randomly branched, chemically reactive, clustering polymers, and, therefore, thermoplastic modeling concepts are only partially applicable.

Here, we investigate the effect of the molecular rearrangement induced by an extensional flow on the ultimate strength and ductility of thermoset fibers, and the dependence on the extent of polymer reaction (curing). As will be seen, our recent work on stiffness modeling [13] serves as a baseline for the current study. We describe how the stretching of the polymer molecules by the flow affects the mechanical properties of the solid fiber, and present power law relationships between these properties and the fiber diameter. The observed fibers' ductility is explained by a condition for brittle-ductile transition at small size scale. The theoretical modeling is corroborated by experimental results from tensile tests of epoxy fibers. Details on the experimental materials and methods may be found in Appendix B and in our previous publications [6,8,10,13].

2. Molecular conformation under extensional flow: background

The key to achieving high fiber stiffness and strength lies in the processing of the resin, whether neat or dissolved in a solvent, prior to drawing by an extensional flow. Throughout the curing process of a thermoset polymer resin, the individual monomers progressively bind together, forming intricate clusters similar to branching trees. Each such cluster is a single polymer molecule. This branching phenomenon arises when segments of reacted polymer chains interconnect (crosslink) through covalent bonding.

As the curing process proceeds, these clusters steadily increase in size until reaching a critical juncture known as the gel point. At this pivotal stage, the first infinite cluster emerges, permeating (percolating) the entirety of the polymer system and marking its transition from a liquid to a solid state. Approaching the gel point, while the polymer solution is still fluid, the clusters exist in a state of marginal overlap with neighboring clusters. This separation between clusters prevents extensive overlapping, which could trigger chemical reactions leading to the formation of larger clusters (see illustrations in Fig. 2) [28]. In that sense, thermosets are distinct from thermoplastics, as the latter form a less compact, entangled network of linear chains [12,27]. The cluster's degree of polymerization (number of monomers, N) is a crucial variable that determines the polymer rheology and its conformation under extension.

The polymer conformation in extensional flow is governed by two competing processes: (i) a constant strain rate (velocity gradient), s [$\sec^{-1}$] [12,29], whether applied mechanically [6] or electrically [8]; (ii) the cluster relaxation time, τ [sec], that is, the time to return from a stretched, stressed state to equilibrium, relieved state. The competition is between two time rates, that of the strain and that of the relaxation. As the curing reaction proceeds, clusters grow (larger N) and their relaxation time is longer because of higher viscosity (refer to first subsection in Appendix A) [13]. High strain rate combined with slow relaxation result in high molecular extension and orientation, because the polymer does not have sufficient time to relax and therefore remains extended. Conversely, low strain rate combined with fast relaxation result in coiled, relieved state in which chain sections are arbitrarily oriented.

A sharp transition in molecular extension and orientation is seen at a critical strain rate, $s_c = \tau^{-1}$ [13], a phenomenon characteristic of polymer solutions in fast extensional flows [19]. At strain rates lower than s_c, the polymer extension is negligible, whereas above s_c the extension rises steeply with increasing strain rate. Close to the gel point, the degree of polymerization is high and therefore relaxation is slow (large τ), so that the extension transition occurs at lower strain rates and the likelihood of the desirable high extension is higher [6,8,10]. Molecular orientation and elongated nodular structure are evidenced by polarized Raman spectroscopy and plasma-etching of electrospun fibers (Fig. 2), respectively [13].

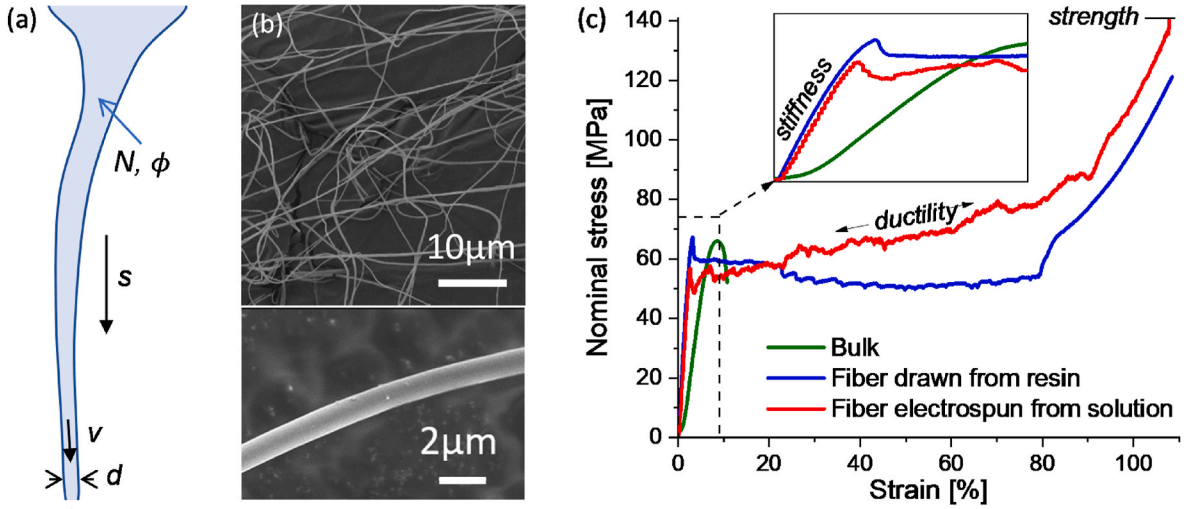

Fig. 1. Epoxy fibers prepared by extensional flow. (a) Illustration of extensional flow at strain rate s of polymer solution of concentration ϕ and degree of polymerization N. (b) SEM images of electrospun epoxy fibers. (c) Typical stress-strain plots of fibers obtained by mechanical and electrical drawing of epoxy resin or solution, respectively, compared to bulk epoxy [6,8]. The unique mechanical properties – elastic stiffness, ultimate strength, and plastic ductility - are indicated. Nominal stress is used (tension force divided by the cross-sectional area of the fiber before deformation); the true ultimate strength is about twice the nominal strength.

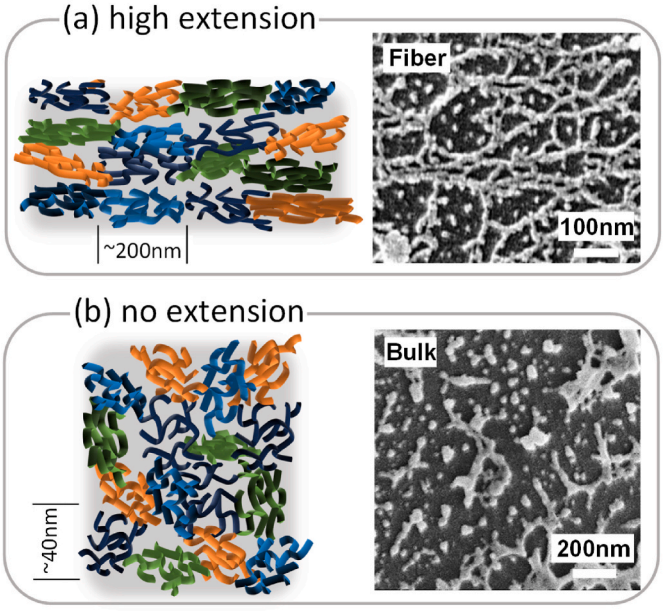

Fig. 2. Polymer conformation under extensional flow. (a) Packing illustration of marginal overlapping, extended polymer clusters (colored) in solution of smaller polymer molecules (gray background). On the right, corresponding nodules (solidified clusters) in plasma-etched electrospun epoxy fibers, showing nodules alignment with the fiber direction (horizontal). (b) Clusters' arbitrary arrangement in bulk epoxy. Cluster size order of magnitudes are denoted. Adapted from ref. [13].

Given the extension and molecular orientation of a cluster, its stiffness and ultimate strength are modeled, both exhibiting a steep rise beyond the critical strain rate. Under these conditions, the cluster's modulus and strength are proportional to the flow strain rate, s, applied during fiber preparation (see justification in Appendix A). Some of that extension is retained in the solid fiber, leading to the fiber's overall average stiffness (elastic modulus) and ultimate strength, approximated by:

$$\begin{matrix} E \approx E_0 p_c s/s_c \\ \sigma \approx \sigma_0 p_c s/s_c \end{matrix} \quad s \gg s_c \tag{1}$$

where E_0 is the reference modulus of bulk polymer, σ_0 is the reference bulk strength, and p_c is the critical extent of reaction (the fraction of clusters, explained below). E_0 and σ_0 are independent of p_c because the bulk polymer is amorphous and isotropic and does not contain stretched clusters, see Equation (A2) in Appendix A. We see that the modulus and strength depend on the dimensionless ratio $s/s_c = s\tau$, which reflects the competition between the applied strain rate and the relaxation time: when both are high, the modulus and strength will be high; when both are low, the properties are expected to remain as in bulk.

The parameter p_c indicates the fraction of reacted bonds out of all possible bonds, near the gel point. These reacted bonds are mostly in large clusters, which dominate the stiffness and strength of fibers formed at high strain rates; the contribution of small clusters and free monomers to the stiffness and strength is relatively negligible because of their fast relaxation. For example, in a system with bifunctional monomers and trifunctional crosslinkers, such as epoxy, each monomer links to two others from each of its two ends (that is, chemical functionality of 4), and its corresponding critical extent of reaction is $p_c = \frac{1}{4-1} = 0.33$; this means that at the gel point just about a third of all possible bonds are activated, and the complementary fraction $1 - p_c$ is bonded afterwards [10]. Processing the polymer as close to the gel point as feasible (large clusters, slow relaxation) and at a high strain rate may result in stiffer and stronger fibers. Evidently, at extremely high strain rates, the stiffness and strength of maximally extended chains is bounded by the stiffness and strength of the covalent bonds.

Equation (1) captures the fundamental physical mechanisms underlying the unique properties of epoxy fibers. These include the intensity of the stretching induced by extensional flow, which results in aligned molecular conformation; the competing relaxation of the polymer molecules, which tends to relieve that alignment; and the extent of the bonding reaction in a thermoset polymer, which determines the fraction of aligned molecules. The subsequent sections on stiffness, strength, and ductility use this paradigm as their baseline.

3. Fiber stiffness and diameter dependence: summary

In our most recent work we presented experimental data for the stiffness (elastic modulus)-diameter dependence of epoxy fibers prepared by extensional flow using various techniques and material compositions, supported by theoretical arguments (Fig. 3) [13]. Here, we briefly recount these results as they are pertinent to our new developments and results for strength and ductility dependencies on fiber diameter, which are presented in the next sections.

The modulus dependence on the strain rate when the strain rate is high is given in Equation (1), $E \sim s$. In a volume conserving flow with a constant strain rate, the diameter dependence on strain rate is $d \sim s^{-1/2}$, because the flow velocity is inversely related to the jet cross sectional area. Further diameter shrinkage may result from tighter packing of aligned molecules, but this is deemed negligible with respect to the shrinkage of the flow diameter. Thus, fibers formed at high strain rates have high modulus and are thinner. Combining both relationships leads to the following fiber diameter-dependent stiffness:

$$E \approx E_0 \left[1 + p_c \left(\frac{d}{d_c}\right)^{-2}\right] \tag{2}$$

where d is the fiber diameter, and d_c is the critical diameter or the crossover diameter below which the modulus rises (see details in Appendix A, Equations (A4) and (A5)). The term 1 is added to account for low strain rates. For fibers above the critical diameter, $E \approx E_0$, whereas below the critical diameter the modulus is proportional to the diameter inverse-squared, $E \sim d^{-2}$. Arguments for this power law are provided in more detail in Appendix A.

The experimental data spans a wide range of fiber diameters of about 2–300 μm; the normalization of the diameters by a suitable critical diameter for each test group enables grouping of all data in a single universal plot as seen in Fig. 3. The values of the critical diameter were obtained by horizontally shifting the experimental data of each test group so that it will best fit the universal curve; the shifting factor is the value of d_c indicated in the figure's legend.

The critical diameter depends on the extent of reaction and on the solution and flow parameters such as polymer concentration, initial diameter, initial velocity, drawing distance, and monomer relaxation time (Equation (A5)) [13]. It is an important concept, implying that the phenomenon of steep rise in stiffness and strength occurs only in fibers with diameters below a certain diameter, but not in fibers with larger diameters. The critical diameter is the consequence of the sharp transition in chain extension at a critical strain rate (described in the previous section) characteristic of polymers in fast extensional flows. In other words, the rise in stiffness and strength which starts at a critical diameter occurs only when, during fiber forming, chains transition to high extension.

The dependence of stiffness on fiber diameter, along with the concept of a critical diameter that defines the domain of stiffness increase, can be extended to the analysis of fiber strength described in the next section. This is because both strength and stiffness are predominantly driven by the same mechanisms induced by the extensional flow: the molecular alignment of clusters and the shrinkage of the diameter.

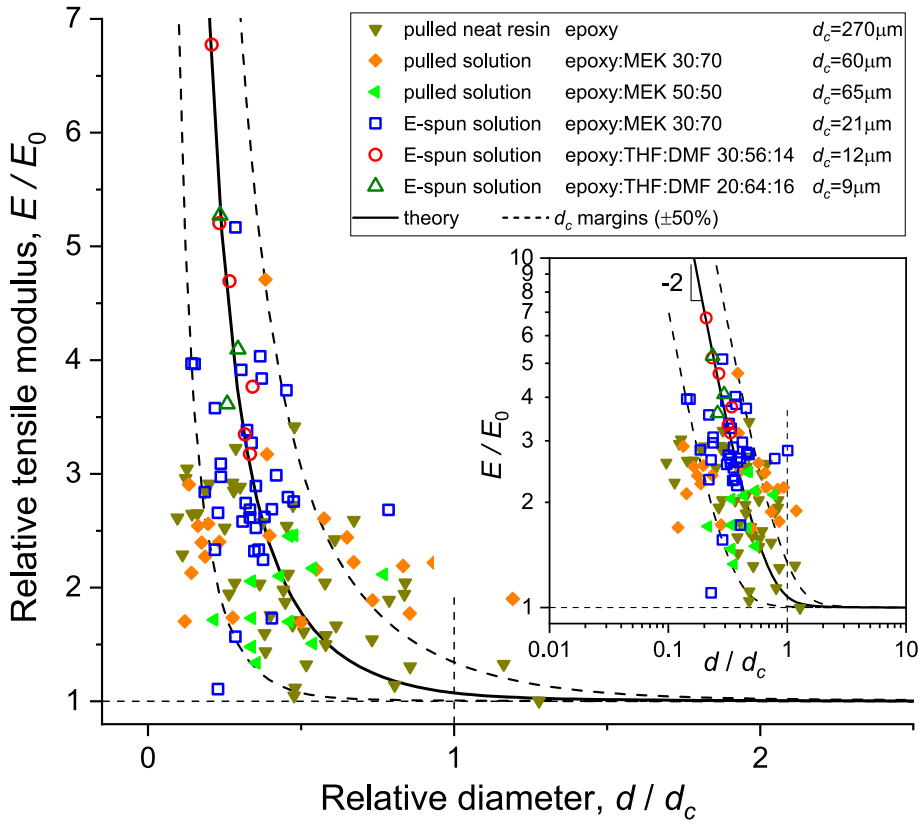

Fig. 3. Fiber stiffness and diameter dependence. Experimental data of mechanically drawn (pulled, solid symbols) and electrically drawn (E-spun, open symbols) epoxy fibers from neat resin or solution at various concentrations and solvent compositions [6,8,13]. The fiber diameter d is normalized by the critical diameter d_c indicated in the legend for each test group. The modulus E is normalized by the modulus of bulk epoxy, E_0 (1 GPa and 0.7 GPa for pulled and electrospun fibers, respectively). The data is compared with the theoretical model. Inset: same data in log-log coordinates, showing the power slope. Adapted from ref. [13].

4. Ultimate strength

4.1. Strength and diameter dependence

The strength diameter-dependence model involves a similar approach as for the stiffness. At high strain rate the cluster strength is proportional to the strain rate, $\sigma \sim s$ (Equation (1)). In a volume conserving flow, the diameter decreases with the inverse square root of the velocity; as the strain rate is constant, the velocity is proportional to the strain rate, and therefore $d \sim s^{-1/2}$. Using these relations, the high strain rate component is obtained. This leads to the following fiber diameter-dependent nominal ultimate strength:

$$\sigma \approx \sigma_0 \left[1 + p_c \left(\frac{d}{d_c}\right)^{-2}\right] \tag{3}$$

where σ_0 is the reference strength in bulk, and the term 1 is added to account for low strain rates. Refer to details in Appendix A, Equations (A1) to (A3) and Equations (A4) and (A5)). Note the similarity of this equation to the stiffness diameter-dependence (Equation (2)): at the scale of a monomer, whose interactions include intramolecular and intermolecular bonds, we may expect proportionality between the strength and the stiffness of these bonds [30,31].

Equation (3) shows that for fibers above the critical diameter, $\sigma \approx \sigma_0$, whereas below the critical diameter the strength is proportional to the inverse-squared diameter, $\sigma \sim d^{-2}$. The ultimate strength is not directly affected by the diameter: this seeming size dependence results from two parallel processes – molecular alignment and diameter reduction – both correlated to the high extension induced by the flow. In this model, fracture mechanics considerations were ignored, as these fibers are highly ductile (Fig. 1c) and notch-insensitive (see Section 5.1).

This strength model is in agreement with epoxy fibers' experimental results. The results, alongside the model, are shown in Fig. 4 for the same test groups as the stiffness and the same corresponding critical diameters. The experimental data spans a wide range of fiber diameters of about 0.4–300 μm and is therefore normalized by the critical diameter of each test group, as done in Fig. 3. The results are striking. The improvement in nominal strength goes up to about 30 times the bulk strength for a fiber of diameter 410 nm and up to about 15 times for fibers above 1 μm. The true strength is on average about twice the nominal strength, $\sigma_{true} \cong \sigma(1+\varepsilon_p)$ where ε_p is the plastic strain (Fig. 1c) – refer to Equations (A6) and (A7) in Appendix A:

$$\sigma_{true} \approx \sigma_0 \left[1 + (1+k_p) p_c \left(\frac{d}{d_c}\right)^{-2}\right] \tag{4}$$

where the left term 1 is added to account for low strain rates. k_p denotes the contribution of the plastic strain to the true strength. The factor $(1+k_p)$ amounts to about 2.04 for the tested epoxy fibers (Fig. 8). Thus, the dependence of the true stress on the relative diameter is the same as for the stiffness, but its slope in epoxy fibers is about twice as steeper.

By comparison, the improvement in modulus is up to about 7 times (Fig. 3), but we note that the modulus measurements were limited to fiber diameters above 2 μm; in fact, the nominal strength rise in fibers of such diameter is similar to the stiffness rise, whereas the true strength rise is about twice the stiffness rise. Critical diameter values for scaling the strength data (Fig. 4 legend) generally corroborate theoretical predictions (refer to Equation (A5) in Appendix A) [13]. Notably, neat epoxy resin exhibits a higher critical diameter due to its concentrated composition and stronger dependence on the polymerization degree. Higher solution concentrations yield larger critical diameters for the

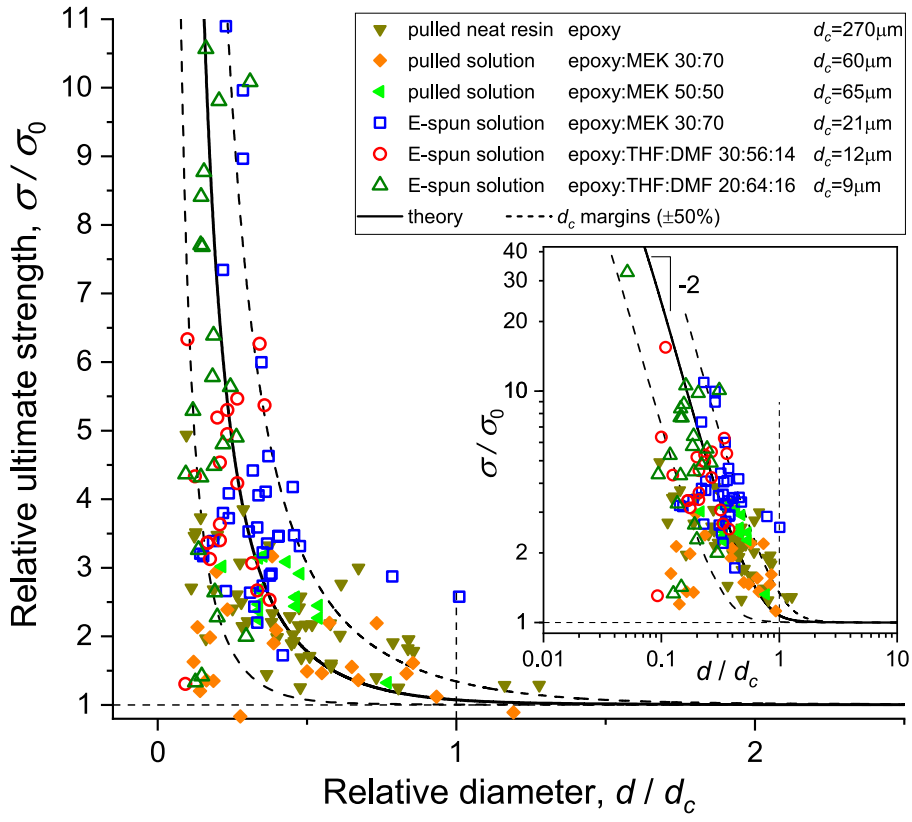

Fig. 4. Fiber nominal ultimate strength and diameter dependence. Experimental data of mechanically drawn (pulled, solid symbols) and electrically drawn (E-spun, open symbols) epoxy fibers from neat resin or solution at various concentrations and solvent compositions [6,8]. The fiber diameter d is normalized by the critical diameter d_c indicated in the legend for each test group. The ultimate strength σ is normalized by the bulk strength σ_0 (35 MPa and 30 MPa for pulled and electrospun fibers, respectively). The data is compared with the theoretical model. Inset: same data in log-log coordinates, showing the power slope. The strength is nominal (engineering stress); on average, the true strength is about twice the nominal strength.

same drawing technique and solvent composition.

Similar to stiffness, the strength results involve a wide range of processing parameters, among them the polymer type, solution concentration, temperature, and extent of reaction [6,10], which can be tuned to achieve desired properties. The drawing strain rate may be controlled by the electric field [8] or the pulling speed [6], so long as it is confined to the bounds imposed by the jet strength [32]. Different solvent compositions and additives like salt [33] may be used to enhance electrical conductivity and, consequently, the applied stress.

4.2. *Strength enhancing mechanisms: discussion*

The fact that the experimental strength data converges into the prediction of Equations (3) and (4), using the same process conditions and critical diameters as for the stiffness, implies that similar physical mechanisms enact the stiffness and strength, that is, molecular stretching and orientation. Furthermore, the true stress model in Equation (4) may suggest that the effect of the plastic deformation induced by the cold drawing leading to fracture is added via the prefactor k_p on top of the flow-induced stretching and orientation. This outcome is supported by the large overall draw ratio (Fig. 1c) and the high molecular orientation measured in necked fibers after cold drawing [9]. Two possible mechanisms to justify this outcome are proposed: (i) Cold drawing induces orientation in both the clusters, which are pre-elongated by the extensional flow, and the amorphous region whose pre-elongation vanishes due to very fast relaxation. However, the molecular structure of the amorphous region resembles the rigid structure of bulk epoxy, which forms a 3D isotropic network of bonded monomers with chemical functionality of about 4 (that is, each monomer bonds covalently with four neighboring monomers) [10]. Therefore, even if some of these bonds dissociate by substantial plastic deformation, the amorphous part is less likely to incur molecular reorientation. By contrast, the molecular structure of the clusters (Fig. 2a) is amenable to further stretching and reorientation. This is expected even if the clusters incur some relaxation, as the network structure is imprinted during the flow phase. (ii) During the strain hardening phase of the cold drawing, rearrangement of weak intermolecular bonds (typical of yielding) is exhausted so that overstretched chains will tear when covalent bonds are overstressed, and some further rearrangement will occur. The clusters' pre-elongated network described in Section 5.3 and shown in Fig. 2a is less prone to such rupture as it is more likely to slip under stress. By analogy, the polymer structure resembles a fiber-reinforced composite, where the elongated, chained clusters may represent reinforcing fibers and the amorphous polymer the matrix (bulk). Their fractions in the material near the gel point are p_c and $1 - p_c$, respectively, determining the overall strength.

A complementary question is why is the yield strength almost independent of the fiber diameter. Why is it not described by a relationship similar to Equation (3)? Yield in polymers is usually modeled either as a viscoelastic process (Eyring model), which depends on strain rate and temperature, or as a process similar to crystalline dislocations and disclinations in metals (Young model) [34]. In both models, yielding is dominated by weak intermolecular bonds, which enable polymer rearrangement without breaking covalent bonds. Therefore, even if the polymer is pre-oriented, there is sufficient inter-chain mobility, and the yield strength does not rise. However, once inter-chain mobility is depleted, chains are 'locked' and strain hardening occurs, making in-chain elasticity the dominant mechanism [34,35].

The analysis and discussion of fiber strength are closely related to the analysis of fiber ductility described in the next section, particularly

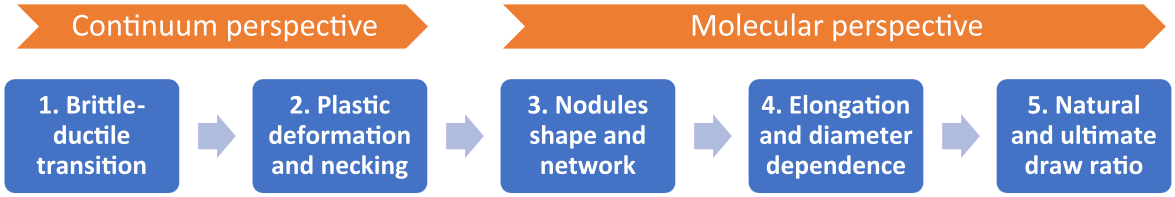

Fig. 5. Ductility perspectives and questions. The following research questions highlight the different aspects of the fibers' outstanding ductility: (1) Why do the fibers become ductile? (2) What is the mechanism driving the plastic deformation? (3) How does the nodular supramolecular structure enable ductility? (4) Does the plastic elongation depend on fiber diameter? (5) Is the plastic draw ratio a material property?

because these thermoset fibers undergo prolonged plastic deformation, resulting in structural rearrangement and strain hardening and, consequently, increased strength.

5. Ductility and supramolecular structure

A spectacular phenomenon in epoxy fibers is their outstanding ductility, atypical of thermoset polymers. Whereas in bulk there is almost no plastic deformation before fracture, these thermoset fibers exhibit about 100 % plastic strain under load (Fig. 1c). Ductility has a major impact on material toughness, that is, its capacity to absorb energy under load before breaking. For example, calculating the energy dissipated during deformation by integrating the area under the stress-strain plots in Fig. 1c, we get energy density of about 75 J m^{-3} in fibers compared to only about 5 J m^{-3} in bulk. Thus, the processing of the fibers via extensional flow causes a generally brittle class of materials to become ductile and tough, a brittle-ductile transition. This transition may be explained through two perspectives: (i) the continuum perspective and (ii) the molecular perspective. The schematic shown in Fig. 5 presents the issues and questions described in the following subsections.

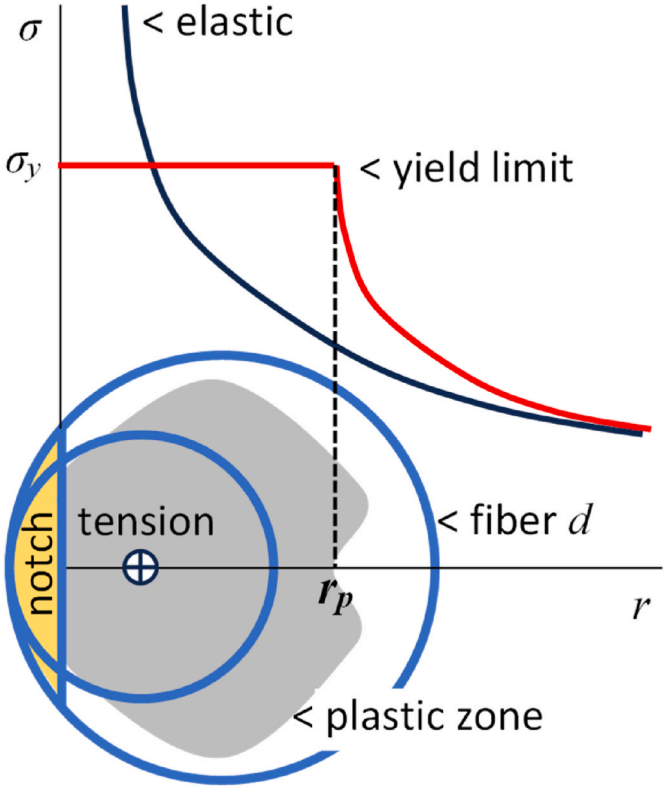

Fig. 6. Fiber Plastic zone size. Illustration of notched small and large fibers (two blue circles) under axial tension perpendicular to the image plane. The yield strength σ_y caps the theoretical elastic stress developing from the notch tip, resulting in a plastic zone (gray area) of width r_p which supersedes the diameter of the smaller fiber. (For interpretation of the references to color in this figure legend, the reader is referred to the Web version of this article.)

5.1. Brittle-ductile transition

Brittle-ductile transition is well-known in glassy, thermoplastic polymers [34,36]. The most straightforward approach, initially developed by Irwin, is crack tip plasticity, which accounts for the plastic zone developing near the tip of a crack in an object under stress. The plastic zone develops in regions where the stress, σ, theoretically diverging to infinity at the tip of a sharp crack, exceeds the material yield strength, σ_y. The plastic zone size r_p in a fiber (illustrated in Fig. 6) is calculated in Appendix A as function of the modulus for a material with known fracture toughness K_{Ic} (Equation (A8)). The dependence on the modulus, $r_p \sim \left(\frac{E}{E_0}\right)^2$, arises from the increase in fracture toughness as a result of higher longitudinal modulus and fracture energy, and can be replaced by dependence on fiber diameter (using Equation (2)), resulting in the plastic zone size as function of the diameter:

$$r_p \approx r_{p0}\left[1 + p_c\left(\frac{d}{d_c}\right)^{-2}\right]^2, r_{p0} = \alpha\left(\frac{K_{Ic0}}{\sigma_{y0}}\right)^2 \quad (5)$$

The subscript 0 denotes bulk properties, and α is a pre-factor unique to the loading type, 0.7 for plane-stress fracture (Mode I), obtained by the theory of brittle-ductile transitions [34,37]. r_{p0} is the plastic zone size in bulk polymer, and the term in squared brackets is a correction factor for fibers prepared by extensional flow.

r_p represents the critical size of the plastic zone, which marks the transition from brittle to ductile failure and the emergence of plastic flow. A fiber with a large diameter d might still break in a brittle manner if it has a sizeable elastic region, but a thin fiber will deform plastically if its entire cross-section or most of it has yielded. So, the condition for fully plastic deformation of a fiber is $r_p > d$, regardless of the notch or defect size and shape (provided it is small relative to the fiber diameter). When is this condition met in a thermoset fiber? Taking epoxy as an example, its yield strength is $\sigma_{y0} \sim 70$ MPa and its fracture toughness is $K_{Ic0} \sim 0.67$ MPa $m^{0.5}$ [38,39], and so the plastic zone in bulk is $r_{p0} \sim 65$ μm.

However, in a fiber produced by strong extensional flow, the critical size for brittle-ductile transition is dependent on the fiber diameter as a result of the molecular anisotropy: the plastic zone size becomes larger by the factor $\left(\frac{d}{d_c}\right)^{-4}$ at diameters smaller than the critical diameter, instating a strong inverse dependence on the fiber diameter via a power law with exponent −4. In the epoxy example, the plastic zone size would be $r_p > 350$ μm for fibers with diameter $d < 0.5d_c$, which encompasses most of the fibers in our tests (Fig. 3), exceeding by far the fiber diameters in this subset; for fibers with diameter $d \cong d_c$, $r_p \cong 115$ μm, so that even the thickest fibers in our tests with a diameter of about 300 μm have a substantial plastic zone.

This assessment demonstrates that for fibers below the critical

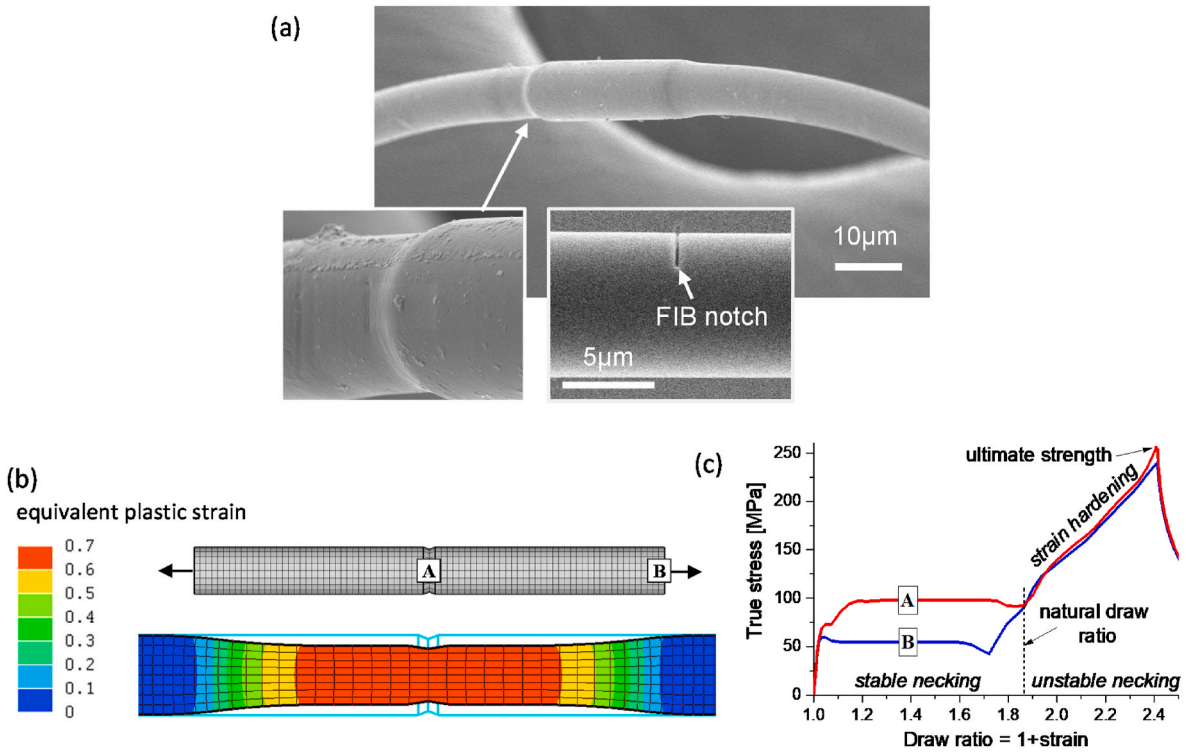

Fig. 7. Fiber plastic deformation and necking. (a) SEM images of a notched epoxy fiber with multiple necking fronts. The neckings did not start at the notch induced by FIB (focused ion beam). (b) Plastic deformation in a fiber near the necking region: finite element simulation using an example of epoxy fiber elastic-plastic properties. (c) Simulated true stress vs. drawing ratio in the fiber center and edge, marked A and B, respectively, showing regions of stable and unstable necking. The draw ratio is the deformed length divided by the original length.

diameter, the entire fiber cross-section (or at least a large part of it) may be within the plastic zone of the crack tip, making the fiber notch-insensitive and enabling the observed long plastic deformation described in the next section.

5.2. Plastic deformation and necking

The plastic deformation in such fibers appears as a necking process: starting from a weak point, a yield zone propagates along the fiber, leaving behind it a fiber section of smaller diameter. Necking is an instability phenomenon in which the loading stress remains constant under continuing deformation [34]. An example of multiple necking fronts in an electrospun epoxy fiber is shown in Fig. 7a, demonstrating insensitivity to an induced notch. A finite element simulation of necking is presented in Fig. 7b, attesting that the plastic strain at the necked section (red region) is uniform and constant during the stable phase and that no yielding occurred outside the neck.

The natural draw ratio in this example is about 1.87 (Fig. 7c), marking the region of stable necking beyond which the whole fiber has necked and instability incurs (strain hardening started). The commonly used term 'natural draw ratio' implies that it is a material characteristic, not the drawing imposed. As volume is conserved during plastic deformation, the diameter is inversely related to the square root of the elongation, and therefore the corresponding neck diameter is about $\frac{d}{\sqrt{1.87}}$. The plastic flow during yielding and cold drawing occurs as local rearrangement of chain sections between crosslinks, rather than long-range movement of molecules [34]. In the necking process, yielding occurs locally at the neck front.

Thus far, the description of the fibers ductility has been largely phenomenological, focusing on the conditions for plasticity and the deformation mechanism. The next section extends the analysis to the molecular scale, examining the impact of extensional flow on the molecular conformation of clusters and the network they form, the resulting enhanced mobility of cluster chains, and the effects on fiber plasticity.

5.3. Nodules shape and network: discussion

The gelation process manifests itself in the solid polymer structure, characterized by the emergence of branched clusters, occupying space but remaining non-interacting with neighbors (Fig. 2b). At the gel point, large cross-linked microgels (clusters) come into contact with neighboring microgels, forming a non-uniform network [40]. Crosslinks continue to form between these clusters as the curing progresses beyond the gel point after fiber drawing. Bulk epoxy has revealed heterogeneous morphology at the nanoscale, showcasing globular nodules of approximately 15–45 nm [40–43], similar in size to the pre-gel clusters (Fig. 2b) [13]. While resembling morphologies are occasionally found in thermoplastic polymers, in the case of epoxy this nodular structure is attributed to its specific curing chemistry, suggesting dense covalent bonding inside the nodules and sparser bonding in the matrix outside. Moreover, a correlation was established between nodule size and various mechanical properties [43]. Recent studies on drawn epoxy fibers indicate low molecular orientation initially, with higher orientation observed in cold-drawn necked fibers due to reorientation caused by plastic deformation [6,9]. This experimental evidence supports the notion that cluster formation during gelation determines the nodular structure post-solidification.

The flow-induced elongated conformation of large clusters significantly influences the nodular structure of solid fibers, affecting bonding rates and cluster interactions. These clusters are oblong, stretched along the fiber axis, and contracted laterally (Fig. 2a). Cluster volume conservation is assumed, as measurements of glass transition temperature indicate only a small difference in free volume between bulk and fibers (see Section 5.4). Consequently, the density of unreacted branch ends at

cluster tips is higher than at the cluster sides. For example, a cluster in a fiber prepared at a relative strain rate of $\frac{\dot{s}}{\dot{s}_c} = 3$ will be elongated by a factor of ~4.5 and its diameter will shrink by a factor of $\sim \sqrt{4.5}$, resulting in an oblong shape with an aspect ratio of about 10 [13]. Plasma etching of epoxy surfaces supports this suggestion, revealing an elongated nodular network generally oriented parallel to the fiber direction (Fig. 2a).

The preference for longitudinal crosslinking between clusters, as a result of their higher tendency to bond with each other at their tips (Fig. 2a), persists even after some relaxation, imprinting (that is, permanently fixing) a specific network crosslinking structure that influences the elastic and plastic behavior of the solid matrix. This network tends to form sequential chains of nodules, enhancing the stiffness, strength, and ductility. The term supramolecular structure in the title of this section relates to this nodular network, as it is a self-assembly of large sub-structures, the nodules. Ductility, atypical of brittle thermoset polymers, is likely enhanced by the higher mobility of chained nodules aligned along the fiber axis compared to the omni-bonded nodules in bulk. In this way, higher ductility should be expected when the stretching and orientation are higher, concurrent with decreasing fiber diameter. When cold drawing is applied to a fiber with molecular pre-orientation, the chained nodules may slide on each other, reminiscent of chain sliding in thermoplastic polymers. This is supported by the observation that the stress during the stable necking phase is fairly constant (Fig. 1c and 7c), implying that intermolecular bonds are dominant, disconnecting and reconnecting as a result of the molecular rearrangement, without affecting the stress. Furthermore, the amorphous regions that are initially isotropic will align through the necking process, and the overall orientation will grow [9].

After reviewing the phenomenological and molecular aspects of fiber ductility in the previous sections, we now focus on modeling the dependence of the plastic strain on fiber diameter and the extent of reaction. This model is based on the concept of chain stretching and alignment induced by extensional flow, consistent with the approach presented in the stiffness and strength analysis.

5.4. Elongation and diameter dependence

The maximum draw ratio $(1 + \varepsilon_p)$ observed in epoxy fibers experiments is slightly above 2 (on average) for a wide range of compositions and processing (Fig. 8), with a weak dependence on fiber diameter. The question arises as to why the diameter-dependence of the draw ratio is so different from that of the stiffness and the strength, both rising steeply with decreasing diameter below the critical diameter. Inter-chain slippage and plastic elongation are more likely when molecular orientation is high. Furthermore, chain mobility in epoxy fibers is higher than in bulk due to larger free volume, reflected in the lower glass transition temperature T_g: in fibers pulled from neat resin, T_g dropped from 83 °C in bulk epoxy to 80 °C [6]; in electrospun fibers, which generally have higher molecular pre-orientation, it fell to a lower value of 74 °C [8].

Assuming that, in fibers prepared at high strain rates, the plastic elongation is proportional to the cluster's relative extension at these conditions, we suggest that the plastic strain ε_p may be expressed by (Equation (A6) in Appendix A):

$$\varepsilon_p \approx k_p \left[1 - p_c \left(\frac{d}{d_c}\right)^2\right], d \ll d_c \tag{6}$$

where k_p is the plastic strain proportionality prefactor (measured about 1.04 for the epoxy fibers, Fig. 8). This model predicts the diameter dependence of the plastic strain, as seen in Fig. 8 for the same test groups as the stiffness and strength and the same corresponding critical diameters (Fig. 3, legend). The data is quite scattered, because, in some of the tests (particularly at small diameters), the fibers broke before the necking completed its propagation along the full fiber length. This may account for the slight drop in the plastic strain of fibers with low relative diameter, $\frac{d}{d_c} \lesssim 0.2$, seen in Fig. 8. That said, a clear trend is observed: for typical values of the diameter below the critical diameter, the plastic strain grows moderately with decreasing diameter and saturates into a constant value slightly above 1 on average.

The question why the plastic strain diameter-dependence is only moderate may be addressed by the following argument. In the stiffness and strength rise, the dominant mechanism is molecular orientation of

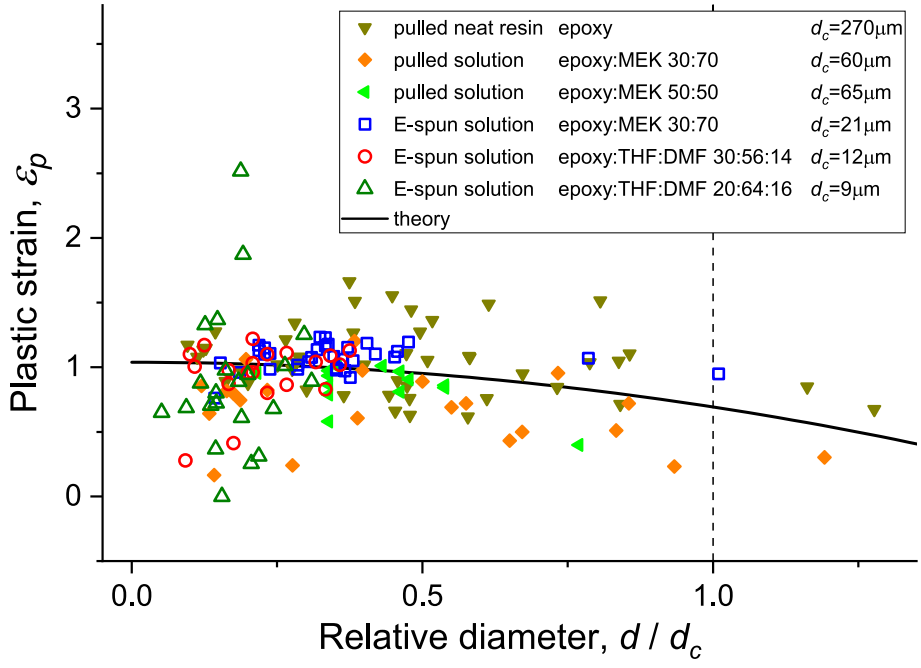

Fig. 8. Fiber plastic strain and diameter dependence. Experimental data of mechanically drawn (pulled, solid symbols) and electrically drawn (E-spun, open symbols) epoxy fibers from neat resin or solution at various concentrations and solvent compositions [6,8]. The fiber diameter d is normalized by the critical diameter d_c indicated in the legend for each test group. The data is fitted to the theoretical model (Equation 6) with a prefactor k_p of 1.04.

chain segments. To overcome the dominant intermolecular weak bonds, the fraction of oriented segments must be very high, and only then can the stiffness and strength rise steeply in proportion to the strain rate. This may be seen in the mixture rule used to assess the stiffness and strength (Equation (A1) in Appendix A). By contrast, to obtain high ductility, such high orientation is not required, as the dominant mechanism is more likely the slippage of chains of clusters and the amount of free volume.

We may ask how universal the described ductility and the model explaining it are. In the next section, we will put these results in perspective using the concept of natural draw ratio and examine whether this behavior can be considered a material property shared by these fibers, with its origin in the molecular structure induced by extensional flow.

5.5. Natural and ultimate draw ratio

The literature on the natural draw ratio suggests dependence on initial molecular orientation [34,44–46]. For example, the natural draw ratio of cold-drawn polyethylene terephthalate fibers of different initial birefringences (molecular orientation) decreased with increasing pre-orientation. It was proposed that the maximum possible stable draw ratio is determined by the network limiting extensibility for a given polymer network, which is a function of the network's original geometry and linkages [34,44]. The limiting extensibility is reached when the polymer chains are stretched to the maximum possible, that is, all monomers are perfectly aligned in the stretching direction. According to this theme, when pre-orientation is induced during fiber formation, the remaining extensibility is shorter than when such pre-orientation does not exist, resulting in smaller natural draw ratio in fibers with larger pre-orientation.

By contrast, experimental results of mechanically and electrically drawn epoxy fibers show that the natural draw ratio has a relatively fixed value of nearly 2, rising moderately with fiber diameter reduction [6,8]. These results imply that, even if the nodules' limiting extensibility was reached, these fibers remained ductile somewhat further, possibly due to the mobility of chains of nodules. In other words, the polymer system has two scales of extensibility, the molecular scale of the individual nodules and the supramolecular scale of the nodular network. The overall extensibility is likely a merging of both. Molecular orientation measurements, carried out by Raman spectroscopy and X-ray scattering [6,9,13], as well as recent Raman tests of near-micron fibers (to be published), indicate an incipient trend of increasing pre and post orientation with decreasing fiber diameter.

The draw ratio is $1+\varepsilon_p$, including the natural draw ratio and the proceeding deformation during the strain hardening (Fig. 1c and 7c). The experimental data shows that the natural draw ratio corresponds to the overall draw ratio and is slightly below it, so that we may project that the model in Equation (6) applies to the natural draw ratio as well, though with a lower prefactor. The natural draw ratio may be isolated by using the ratio between the neck diameter and the fiber diameter, inverse-squared, or $(d_{neck}/d)^{-2}$, assuming volume conservation during cold drawing. This is demonstrated by measuring the necked diameter of electrospun epoxy fibers (Fig. 9): although the plastic strain data is widely scattered, and although the true ultimate strength in this test group spans a wide range from 90 MPa to 1600 MPa (Fig. 4) reflecting a wide range of molecular orientation, the neck diameter remains linearly dependent on the fiber initial diameter, and the natural draw ratio hardly varies (on average) with the diameter. This points at a material property shared by the fibers in this test group, whose origin is in the molecular structure induced by the extensional flow.

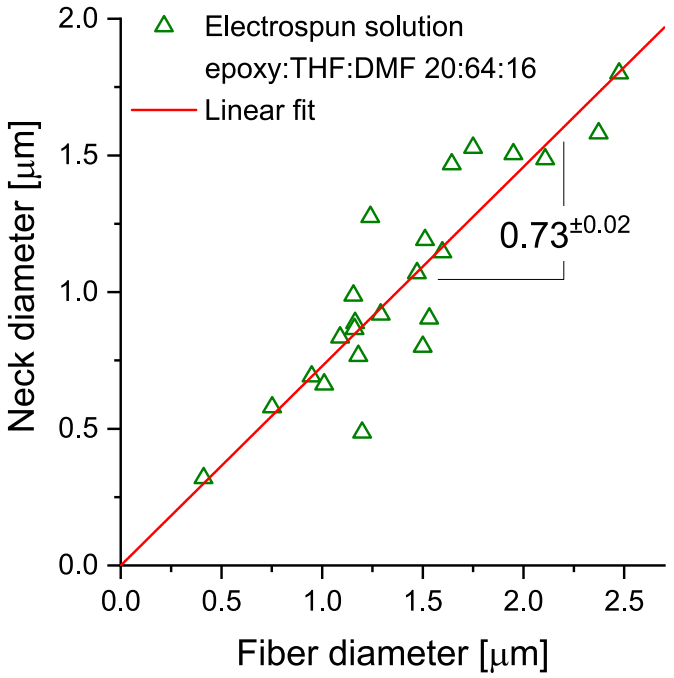

Fig. 9. Necked diameter vs. initial fiber diameter. Fibers electrospun from 20 % epoxy solution dissolved in 80 %:20 % THF:DMF (the open triangle test group in Fig. 8). Tensile testing conducted in a SEM (scanning electron microscope). The indicated slope corresponds to a natural draw ratio 1.88 ± 0.10 (volume conservation assumed).

6. Conclusions

When a thermoset polymer resin or solution is subjected to extensional flow by mechanical or electrical drawing, the resulting micro and nanofibers demonstrate marked enhancements in mechanical properties, making them promising candidates for diverse applications. The stiffness, strength, and toughness of these fibers are size-dependent, growing steeply below a characteristic critical fiber diameter. This study explores the molecular behavior of epoxy resin, a typical thermoset polymer, under extensional flow. It proposes a theoretical model linking mechanical properties to material composition, curing reaction extent, and flow conditions.

During extensional flow, the diameter of the liquid jet narrows down while, at the same time, branched polymer molecules (clusters) are strongly stretched and oriented. When a characteristic critical strain rate is exceeded, large elongated clusters do not have time to relax, and their extended conformation and anisotropic bonding are mostly retained after solidification. The result is a network of clusters generally oriented in the fiber direction, with high bonding density in that direction. Consequently, stiffness (elastic modulus), ultimate strength, and ductility steeply increase in the fiber direction. As the stiffness and strength are strain rate-dependent, an inverse-square power law is found that correlates between them and the diameter, asserting their size-dependence. The fibers exhibit remarkable ductility, which is atypical of thermoset polymers, caused by the aligned molecular conformation, the nodular network, and the brittle-ductile transition at small size.

The tensile experiments on epoxy fibers prepared by mechanical and electrical drawing from different material compositions appear to confirm the proposed model. Based on this scheme, desired fiber diameter and tensile properties may be obtained by tuning the material composition, the degree of curing, and the flow strain rate. Thermoset

micro and nanofibers generated by extensional flow may find applications such as reinforcement in composite materials and benefit from the intrinsic chemical and physical properties of thermosets.

Funding

This research received no external funding.

CRediT authorship contribution statement

Israel Greenfeld: Writing – review & editing, Writing – original draft, Visualization, Validation, Project administration, Methodology, Investigation, Formal analysis, Conceptualization. **Mark Shneider:** Writing – review & editing, Validation, Investigation, Data curation. **Ulyana Shimanovich:** Writing – review & editing. **H. Daniel Wagner:** Writing – review & editing, Supervision, Resources, Project administration, Funding acquisition, Conceptualization.

Declaration of competing interest

The authors declare that they have no known competing financial interests or personal relationships that could have appeared to influence the work reported in this paper.

Acknowledgments

The authors would like to acknowledge support from the G.M.J. Schmidt Minerva Centre of Supramolecular Architectures at the Weizmann Institute, and the generosity of the Harold Perlman family. This research was supported by a research grant from the Tom and Mary Beck Center for Advanced and Intelligent Materials, as well as by the Ilse Katz Institute for Material Sciences and Magnetic Resonance Research, at the Weizmann Institute of Science, Rehovot, Israel.

Appendix A. modeling details

Strain rate dependence

At strain rates beyond the critical strain rate, the cluster's modulus and strength are proportional to the flow strain rate applied during fiber formation. This simple relation may be justified by the following argument (the theoretical treatment is provided in Ref. [13]): The flow strain rate, s, elongates the cluster to a relative extension, ϵ, defined as the ratio between the cluster stretched size and its maximal possible extension (when all monomers co-align). Thus, from the top end of a cluster to its far end downstream, the flow incurs a velocity difference equivalent to the product of the cluster length (or extension) by the gradient (strain rate). Consequently, the cluster tends to extend at a rate proportional to ϵs as a result of the hydrodynamic friction force acting on it.

However, at the same time, the extension induces an entropic elastic force, f, which tends to retract the cluster back to relaxed state within a relaxation time τ. Thus, the retraction rate is proportional to f/τ. The cluster's resulting extension rate is the difference between the two rates, that is $\dot{\epsilon} \approx \epsilon s - f/\tau$. In a steady flow, the relative extension is stable (its time derivative is zero), so that the extension and retraction rates reach equilibrium rapidly and become equal. Equating both rates and rearranging, $f/\epsilon \approx s\tau \approx s/s_c$, remembering that the critical strain rate is inversely related to the relaxation time, $s_c = \tau^{-1}$. The ratio f/ϵ is the stiffness of a stretched cluster, an analog of a spring constant, force divided by extension. The cluster stretched conformation is partially retained after solidification, and therefore the ratio f/ϵ represents the cluster's stiffness and strength in a solid fiber. The overall stiffness and strength of a solid fiber correspond to those of the clusters, and are therefore proportional to the strain rate, that is, $E \sim s/s_c$ and $\sigma \sim s/s_c$.

The equation $f(\epsilon) \approx \epsilon s\tau$ derived above is the stretching equation, whose solution yields the extension as a function of the strain rate and relaxation time. The dimensionless entropic force $f(\epsilon)$ is linear at small extensions, but rises sharply at high extensions as chain conformations become less probable. An example of the nonlinear force function at high strains is $f \approx \frac{3\epsilon}{1-\epsilon}$, which, when substituted in the stretching equation, yields the extension at high strain rate, $\epsilon \approx 1 - \left(\frac{s}{s_c}\right)^{-1}$, where $s_c = 3/\tau \approx \tau^{-1}$ [13]. The extension expression is used later on (Equations (A2) and (A6)) to derive the strength (and stiffness) and plastic strain dependencies on the relative strain rate s/s_c.

The relaxation time of a cluster, that is a single branching molecule in the pre-gel state, is known via Rouse and Zimm models, $\tau \approx \tau_0 N^x$, where N is the cluster's degree of polymerization and x is 1.8 for neat resin and 1.2 for solution. $\tau_0 \approx \eta b^3/kT$ is the monomer relaxation time, where η is the medium viscosity, b is the monomer length, k is Boltzmann constant, and T is the temperature [13]. The degree of polymerization is given by $N \approx \left|\frac{p-p_c}{p_c}\right|^{-2.22}$, where the extent of reaction p of the liquid resin or solution, prepared for drawing by extensional flow, can be measured by infrared spectroscopy [10,13]. Near the gel point, the degree of polymerization rises sharply with the extent of reaction and consequently the relaxation time becomes long, resulting in high extension and high stiffness and strength. This explains the advantage of tuning the solution reaction close to the gel point prior to fiber preparation.

Stiffness and strength

The cluster's structure is represented in the model as an aggregate of monomers [12,47,48], each with strength and stiffness related to its orientation with respect to the fiber's main axis: monomers aligned with the fiber transmit the longitudinal stress along their backbone, which has high strength and stiffness due to covalent bonds; monomers aligned laterally transmit the longitudinal stress via their interaction with other monomers, which has low strength and stiffness due to weak intermolecular bonds (e.g. van der Waals). The overall fiber strength and stiffness are obtained by a mixture rule of the strengths and stiffnesses of all monomers [13]. More precisely, for stiffness we sum up the compliances (that is, E^{-1}) of all elements along the fiber, whereas for strength we sum up the weaknesses (that is, σ^{-1}). Therefore the overall strength and stiffness are dominated by the weaker and more compliant intermolecular bonds.

The proceeding analysis is developed for the strength, but is equally applicable to the stiffness by replacing the strength symbol σ by the stiffness symbol E. The strength of a cluster is calculated by a mixture rule:

$$\sigma_{cluster} = \left(\frac{P_{\parallel}}{\sigma_1} + \frac{1 - P_{\parallel}}{\sigma_2}\right)^{-1} \tag{A1}$$

where $P_{\parallel}$ is the probability that a monomer will be oriented in the fiber longitudinal direction. Here, iso-stress is assumed, that is, uniform stress throughout the cluster. The strengths σ_1 and σ_2 represent the strength along the monomer backbone (covalent bonds) and across it (intermolecular bonds), respectively, where typically $\sigma_1/\sigma_2 \sim 10^2 - 10^3$ [12,30,31,49].

Under high stretching, the fraction $P_{\parallel}$ may be approximated by the relative extension ϵ, so that $P_{\parallel} \cong \epsilon \approx 1 - \left(\frac{s}{s_c}\right)^{-1}$ (see previous sub-section) [13]. Thus, in the domain of strain rates above the critical strain rate, the overall average strength is approximated by Equation (A1) ($\sigma_1 \gg \sigma_2$):

$$\sigma \approx \sigma_0 p_c \frac{s}{s_c}, s \gg s_c \tag{A2}$$

$\sigma_0 = \frac{3}{2}\sigma_2$ is the bulk strength, dominated by the intermolecular strength, obtained by using $P_{\parallel} = 1/3$ (isotropic). The factor p_c is added to reflect the fraction of the high-strength component (the elongated clusters) while neglecting the contribution of the amorphous component. The theoretical maximum is $\sigma = \sigma_1 p_c$ ($P_{\parallel} \to 1$).

The flow diameter is related to the velocity and hence the strain rate via $d \sim s^{-1/2}$ (volume conservation assumed); tighter packing of aligned molecules may further reduce the diameter, but this effect is assessed as relatively negligible in view of the small difference in free volume between bulk and fibers (see Section 5.4). Similarly, the critical diameter is related to the critical strain rate by $d_c \sim {s_c}^{-1/2}$. This leads to the relation $\frac{s}{s_c} = \left(\frac{d}{d_c}\right)^{-2}$ that, when substituted into Equation (A2), yields the power dependence of the fiber modulus on the diameter:

$$\sigma \approx \sigma_0 p_c \left(\frac{d}{d_c}\right)^{-2}, d \ll d_c \tag{A3}$$

The critical diameter exhibits a power law correlation with the extent of reaction, $d_c \sim {s_c}^{-1/2} \sim N^{x/2}$, characterized by a positive exponent $x/2$ of the degree of polymerization N ($x/2$ is 0.9 for neat resin and 0.6 for solution). Refer to Ref. [13] for details.

Fiber diameter and critical diameter

As the flow is volume-conserving, the flow diameter d decreases with respect to the initial diameter d_0 in proportion to the inverse square root of the velocity ratio v/v_0, where v_0 is the flow initial velocity (feedrate). After solvent evaporation (if diluted), the diameter further decreases with the square root of the polymer volume fraction ϕ. The flow terminal velocity is $v = sl$ for a constant strain rate, where l is the drawing distance, leading to the following relation [13]:

$$d \approx d_0 \left(\frac{\phi v_0}{sl}\right)^{1/2} \tag{A4}$$

The polymer stretch transition in the flow, associated with the stiffness and strength rising transition in the solid fibers, occurs when the flow strain rate equals the critical strain rate, $s = s_c \approx \tau^{-1}$. Thus, the critical diameter is given by:

$$d_c \approx d_0 \left(\frac{\phi v_0}{s_c l}\right)^{1/2} \approx d_0 \left(\frac{\phi v_0 \tau}{l}\right)^{1/2} \tag{A5}$$

where the relaxation time $\tau \approx \tau_0 N^x$ and the degree of polymerization N are given in the first sub-section of this Appendix.

Plastic strain and true strength

Assuming that the plastic strain is proportional to the fraction of cluster monomers initially aligned (before cold drawing) with the fiber direction, and hence to the relative extension ϵ at high strain rates (specified in the first sub-section of this appendix), we suggest that the plastic strain may be expressed by:

$$\varepsilon_p \approx P_{\parallel} \cong \epsilon \approx k_p \left[1 - p_c \left(\frac{d}{d_c}\right)^2\right], d \ll d_c \tag{A6}$$

The critical extent of reaction, p_c, is added to account for the amorphous part that is not initially extended due to fast relaxation. k_p is the plastic strain proportionality prefactor.

The true strength of fibers prepared at high strain rates may be derived by converting the nominal strength (Equation (A3)) using the plastic strain expression:

$$\sigma_{true} \cong \sigma(1 + \varepsilon_p) \approx (1 + k_p)\sigma_0 p_c \left(\frac{d}{d_c}\right)^{-2}, d \ll d_c \tag{A7}$$

where the term $p_c^2 \ll (d/d_c)^{-2}$ was neglected.

Plastic zone size

The elastic stress ahead of a crack tip loaded in plane-stress Mode I is given by linear elastic fracture mechanics, $\sigma \approx \frac{K_I}{\sqrt{r}}$, where $K_I \approx \sqrt{GE}$ is the stress intensity factor, G is the strain energy release rate (fracture energy in a critical crack, G_c), and r is the distance ahead from the tip. Substituting the yield strength, which limits the maximum stress, and solving for r at a critical crack, the plastic zone size (illustrated in Fig. 6) is given by Refs. [36,37]:

$$r_p = \alpha \frac{G_c E}{\sigma_y^2} \cong r_{p0}\left(\frac{E}{E_0}\right)^2, r_{p0} = \alpha\left(\frac{K_{Ic0}}{\sigma_{y0}}\right)^2 \tag{A8}$$

where α is a pre-factor unique to the loading type, and the subscript 0 denotes bulk properties ($\sigma_y \cong \sigma_{y0}$ is assumed). The second term was obtained by assessing the cohesive fracture energy by $G_c \cong \frac{G_{c0}}{E_0}E$, applying the proportionality between the fracture energy and the tensile modulus in brittle materials [49,50].

Appendix B. materials and methods

Following is a brief description of the materials and methods used in this study. Further details may be found in our previous publications [6,8,10,13].

Materials and solutions. The epoxy used was diglycidyl ether of bisphenol-A (DGEBA), resin EP828 (340 g/mol), with hardener EP304 (PolymerG, Israel) in a 100:42 wt ratio. N–N-Dimethylformamide (DMF) and tetrahydrofuran (THF) (Sigma Aldrich) solvents were mixed (2:8 wt ratio) and added to the epoxy, comprising 80 % of the solution weight. DMF (dielectric constant 36.7, boiling point 153 °C) enhanced electrical responsiveness, while THF (dielectric constant 7.6, boiling point 66 °C) aided rapid fiber solidification. The mixture was stirred for 20 min, stored at 55 °C for 294 h, then quenched at −18 °C. Before electrospinning, it was thawed and stirred at 300 rpm for 15 min. Other solvent weight ratios were also tested, as well as methyl ethyl ketone (MEK) (Sigma Aldrich) solvent (see Fig. 3 legend). When neat resin was prepared for pulling tests, it was heated at 80 °C for up to 24 min to approach vitrified state before pulling.

Electrospinning (electrical drawing). The electrospinning system comprised a syringe pump (Fusion 4000, Chemyx) and a DC power supply (Glassman PS/FC50R02). A 21G blunt needle (0.81 mm × 2.5 cm, Covidian, MonoJect) attached to a 10 ml syringe (NORM-JECT) fed the solution at rate 0.5–0.7 ml/h. Fibers were collected on an aluminum net (15 × 15 mm^2 cell) placed 190 mm from the nozzle. A copper rod electrode (100 mm × 2 mm) positioned 10 mm behind the net generated an electric potential of 19–21 kV. Flow rate, electric field, nozzle size, and electrode distance were optimized to minimize bead formation and control fiber diameter. Fibers rested 16 h, were vacuum-treated for 24 h, and cured at 100 °C for 6 h. The fibers were then cut and fixed to a frame.

Pulling (mechanical drawing). A small amount of the mixture was extracted using a 3 × 5 mm spatula tip, and suspended at ~1.5 m height, forming a thinning fiber under gravity at room temperature. Fiber diameter was controlled by adjusting polymer amount and viscosity. Fibers were cured at room temperature for 48 h, then fixed on a frame and post-cured at 80 °C for 5 h. An alternative method was to adhere the liquid drop to one side of the frame and then draw it with the spatula to the other side.

Notching. For fracture toughness tests, a high-resolution FE-SEM with a focused ion beam (FIB) (FEITM Helios NanoLAB 600, Thermo Fisher Scientific) was used to etch a notch in fibers. The fiber was fixed on a silicon wafer and notched along a line of specified length, using Ga^+ ions at 30 kV acceleration voltage and 3 pA beam current. The notched fibers were tested using the same tensile procedure as the un-notched fibers.

Tensile testing. Tensile tests were conducted on an Instron 5965 (UK) with a 10 N load cell. Fiber diameter was measured at three points via optical microscope and averaged. The fiber was clamped, and the frame was removed before testing. A 1 mm/min strain rate was applied until failure, recording force to determine maximum stress and strain at failure, Young's modulus, and toughness. For sub-micron fibers, a custom push-to-pull tensile tester (12.1 N/m cantilever) was designed. Fibers were secured on carbon-taped aluminum foil, and the frame was removed before testing. The device was placed in a SEM (Zeiss LEO Supra 55VP) with a nano-manipulator (Kleindiek, NC-2-3) applying strain at 46 μm/min. ImageJ was used to analyze the cantilever displacement, allowing calculation of the fiber stress and strain.

Data availability

Data will be made available on request.

References

[1] H. Dodiuk, S.H. Goodman, Handbook of Thermoset Plastics Third Edition Introduction, William Andrew Inc, Norwich, NY USA, 2014, pp. 1–12.
[2] C. May, Epoxy Resins: Chemistry and Technology, Marcel Dekker, New York, NY USA, 1988.
[3] J.C. Capricho, B. Fox, N. Hameed, Multifunctionality in epoxy resins, Polym. Rev. 60 (1) (2020) 1–41.
[4] T. Hobbiebrunken, B. Fiedler, M. Hojo, M. Tanaka, Experimental determination of the true epoxy resin strength using micro-scaled specimens, Compos. Appl. Sci. Manuf. 38 (3) (2007) 814–818.
[5] X. Wang, W.J. Zhang, D.G. Yu, X.Y. Li, H. Yang, Epoxy resin nanofibers prepared using electrospun core/sheath nanofibers as templates, Macromol. Mater. Eng. 298 (6) (2013) 664–669.
[6] X.M. Sui, M. Tiwari, I. Greenfeld, R.L. Khalfin, H. Meeuw, B. Fiedler, H.D. Wagner, Extreme scale-dependent tensile properties of epoxy fibers, Express Polym. Lett. 13 (11) (2019) 993–1003.
[7] N. Aliahmad, P.K. Biswas, V. Wable, I. Hernandez, A. Siegel, H. Dalir, M. Agarwal, Electrospun thermosetting carbon nanotube-epoxy nanofibers, ACS Appl. Polym. Mater. 3 (2) (2021) 610–619.
[8] M. Shneider, X.M. Sui, I. Greenfeld, H.D. Wagner, Electrospinning of epoxy fibers, Polymer 235 (2021).
[9] X. Sui, I. Pinkas, H.D. Wagner, A polarized micro-raman study of necked epoxy fibers, Polymer 230 (2021).
[10] M. Shneider, R. Zattelman, A. Kaestner, I. Greenfeld, H.D. Wagner, Electrospinning of epoxy fibers: effect of curing conditions on solution rheological behavior, J. Appl. Polym. Sci. (2023) 1–10.
[11] M. Richard-Lacroix, C. Pellerin, Molecular orientation in electrospun fibers: from mats to single fibers, Macromolecules 46 (24) (2013) 9473–9493.
[12] I. Greenfeld, X.M. Sui, H.D. Wagner, Stiffness, strength, and toughness of electrospun nanofibers: effect of flow-induced molecular orientation, Macromolecules 49 (17) (2016) 6518–6530.
[13] I. Greenfeld, M. Shneider, A. Kaestner, H.D. Wagner, Stiffness modeling of thermoset polymer fibers, J. Polym. Sci. 62 (12) (2024) 2780–2796.
[14] D.W. Mead, R.G. Larson, M. Doi, A molecular theory for fast flows of entangled polymers, Macromolecules 31 (22) (1998) 7895–7914.
[15] L.A. Archer, Polymer disentanglement in steady-shear flow, J. Rheol. 43 (6) (1999) 1617–1633.
[16] V.R. Mhetar, L.A. Archer, A new proposal for polymer dynamics in steady shearing flows, J. Polym. Sci., Part B: Polym. Phys. 38 (1) (2000) 222–233.
[17] S.L. Shenoy, W.D. Bates, H.L. Frisch, G.E. Wnek, Role of chain entanglements on fiber formation during electrospinning of polymer solutions: good solvent, non-specific polymer-polymer interaction limit, Polymer 46 (10) (2005) 3372–3384.
[18] Y.H. Wen, C.C. Hua, Chain stretch and relaxation in transient entangled solutions probed by double-step strain flows, J. Rheol. 53 (4) (2009) 781–798.

[19] P.G. de Gennes, Scaling Concepts in Polymer Physics, Cornell University Press, Ithaca, N.Y., 1979, p. 324.
[20] M. Doi, S.F. Edwards, The Theory of Polymer Dynamics, the Clarendon Press, Oxford University Press, New York, 1986.
[21] D.S. Pearson, A.D. Kiss, L.J. Fetters, Flow-induced birefringence of concentrated polyisoprene solutions, J. Rheol. 33 (3) (1989) 517–535.
[22] H. Watanabe, Viscoelasticity and dynamics of entangled polymers, Prog. Polym. Sci. 24 (9) (1999) 1253–1403.
[23] G. Iannirubertо, G. Marrucci, A simple constitutive equation for entangled polymers with chain stretch, J. Rheol. 45 (6) (2001) 1305–1318.
[24] G.H. McKinley, T. Sridhar, Filament-stretching rheometry of complex fluids, Annu. Rev. Fluid Mech. 34 (2002) 375–415.
[25] P.K. Bhattacharjee, D.A. Nguyen, G.H. McKinley, T. Sridhar, Extensional stress growth and stress relaxation in entangled polymer solutions, J. Rheol. 47 (1) (2003) 269–290.
[26] R.S. Graham, A.E. Likhtman, T.C.B. McLeish, Microscopic theory of linear, entangled polymer chains under rapid deformation including chain stretch and convective constraint release, J. Rheol. 47 (5) (2003) 1171–1200.
[27] I. Greenfeld, A. Camposeo, A. Portone, L. Romano, M. Allegrini, F. Fuso, D. Pisignano, H.D. Wagner, WO(3) nanowires enhance molecular alignment and optical anisotropy in electrospun nanocomposite fibers: implications for hybrid light-emitting systems, ACS Appl. Nano Mater. 5 (3) (2022) 3654–3666.
[28] M. Rubinstein, R.H. Colby, Polymer Physics, Oxford University Press, Oxford, New York, 2003, p. 440, p xi.
[29] I. Greenfeld, K. Fezzaa, M.H. Rafailovich, E. Zussman, Fast X-ray phase-contrast imaging of electrospinning polymer jets: measurements of radius, velocity, and concentration, Macromolecules 45 (8) (2012) 3616–3626.
[30] M.F. Ashby, H. Shercliff, D. Cebon, Materials: Engineering, Science, Processing and Design; North American Edition, 3rd ed.; Butterworth-Heinemann, Oxford, UK, 2013.
[31] F. Ashby, D.R.H. Jones, Engineering Materials 1: an Introduction to Properties, Applications and Design, Butterworth-Heinemann, Oxford, UK, 2011, p. 496.
[32] I. Greenfeld, E. Zussman, Polymer entanglement loss in extensional flow: evidence from electrospun short nanofibers, J. Polym. Sci., Part B: Polym. Phys. 51 (18) (2013) 1377–1391.
[33] X.M. Sui, E. Wiesel, H.D. Wagner, Enhanced mechanical properties of electrospun nano-fibers through NaCl mediation, J. Nanosci. Nanotechnol. 11 (9) (2011) 7931–7936.
[34] I.M. Ward, J. Sweeney, Mechanical Properties of Solid Polymers, third ed., Wiley, Chichester, West Sussex, England, 2013, p. 461.
[35] R.S. Hoy, M.O. Robbins, Strain hardening of polymer glasses: effect of entanglement density, temperature, and rate, J. Polym. Sci. B Polym. Phys. 44 (24) (2006) 3487–3500.
[36] T.L. Anderson, Fracture Mechanics Fundamentals and Applications, 4 ed., CRC Press, 2017.
[37] K.E. Puttick, Size effects in brittle fracture. Proceedings of the 3rd International Conference on Mechanical Behaviour of Materials, Pergamon Press, Oxford, 1979, pp. 11–17.
[38] N. Lachman, H.D. Wagner, Correlation between interfacial molecular structure and mechanics in CNT/Epoxy nano-composites, Compos Part a-Appl S 41 (9) (2010) 1093–1098.
[39] A. Bajpai, A. Alapati, A. Klingler, B. Wetzel, Tensile Properties, Fracture mechanics properties and toughening mechanisms of epoxy systems modified with soft block copolymers, rigid TiO2 nanoparticles and their hybrids, J. Compos Sci. 2 (4) (2018).
[40] C.M. Sahagun, S.E. Morgan, Thermal control of nanostructure and molecular network development in epoxy-amine thermosets, ACS Appl. Mater. Interfaces 4 (2) (2012) 564–572.
[41] U.T. Kreibich, R. Schmid, Inhomogeneities in epoxy resin networks, J. Polym. Sci., Polym. Symp. 53 (1) (1975) 177–185.
[42] K. Dusek, J. Plestil, F. Lednicky, S. Lunak, Are cured epoxy resins inhomogeneous? Polymer 19 (1978) 393–397.
[43] J. Mijovic, J.A. Koutsky, Correlation between nodular morphology and fracture properties of cured epoxy, Polymer 20 (1979) 1095–1107.
[44] S.W. Allison, P.R. Pinnock, I.M. Ward, The cold drawhlg of polyethylene terephthalate, I. C. I. Fibres Ltd. (1965) 66–69.
[45] B.E. Read, J.C. Duncan, D.E. Meyer, Bire|ringence techniques for the assessment O| orientation, Polym. Test. 4 (1984) 143–164.
[46] R. Séguéla, On the natural draw ratio of semi-crystalline polymers: review of the mechanical, physical and molecular aspects, Macromol. Mater. Eng. 292 (3) (2007) 235–244.
[47] R.G.C. Arridge, Mechanics of Polymers, Clarendon Press, Oxford, 1975, p. 246 [Eng.].
[48] I.M. Ward, J. Sweeney, An Introduction to the Mechanical Properties of Solid Polymers, second ed., Wiley, Chichester, West Sussex, England, 2004, p. 382.
[49] M.F. Ashby, Materials Selection in Mechanical Design, fourth ed. ed., Elsevier, Burlington, MA, USA, 2011.
[50] I. Greenfeld, H.D. Wagner, Crack deflection in laminates with graded stiffness-lessons from biology, Bioinspiration Biomimetics 18 (3) (2023).